HIGHER-ORDER DFEM TRANSPORT CALCULATIONS ON POLYTOPE MESHES FOR MASSIVELY-PARALLEL ARCHITECTURES

A Dissertation

by

MICHAEL WAYNE HACKEMACK

Submitted to the Office of Graduate and Professional Studies of
Texas A&M University
in partial fulfillment of the requirements for the degree of

DOCTOR OF PHILOSOPHY

Chair of Committee,	Jean Ragusa
Committee Members,	Marvin Adams
	Jim Morel
	Nancy Amato
	Troy Becker
Head of Department,	Yassin Hassan

May 2016

Major Subject: Nuclear Engineering

ABSTRACT

blah...

DEDICATION

For the Greater Glory of God (AMDG).

"Good ideas are not adopted automatically. They must be driven into practice with courageous impatience. Once implemented, they can be easily overturned or subverted through apath or lack of follow-up - so a continuous effort is required."

- Admiral Hyman G. Rickover

ACKNOWLEDGEMENTS

I would like to thank my graduate advisor and committee chair, Dr. Jean Ragusa for all of his guidance towards the completion of this research endeavour. I would also like to thank my other committee members: Dr. Marvin Adams, Dr. Jim Morel, Dr. Nancy Amato, and Dr. Troy Becker for all of their support.

This research was performed under appointment to the Rickover Graduate Fellowship Program in Nuclear Engineering sponsored by the Naval Reactors Division of the United States Department of Energy.

TABLE OF CONTENTS

Page

LIST OF FIGURES

FIGURE Page

LIST OF TABLES

TABLE Page

1. INTRODUCTION

1.1 Purpose of the Dissertation

1.2 Past Work

1.3 Current Work

1.4 Organization of the Dissertation

The remainder

2. THE DGFEM FORMULATION OF THE MULTIGROUP S_N EQUATIONS

The movement of bulk materials and particles through some medium can be described with the statistical behavior of a non-equilibrium system. Boltzmann first devised these probabilistic field equations to characterize fluid flow via driving temperature gradients [1]. His work was later extended to model general fluid flow, heat conduction, hamiltonian mechanics, quantum theory, general relativity, and radiation transport, among others. The Boltzmann Equation can be written in the general form:

$$\frac{\partial u}{\partial t} = \left(\frac{\partial u}{\partial t}\right)_{force} + \left(\frac{\partial u}{\partial t}\right)_{advec} + \left(\frac{\partial u}{\partial t}\right)_{coll} \tag{2.1}$$

where $u(\vec{r}, \vec{p}, t)$ is the transport distribution function parameterized in terms of position, $\vec{r} = (x, y, z)$, momentum, $\vec{p} = (p_x, p_y, p_z)$, and time, t. In simplified terms, Eq. (2.1) can be interpreted that the time rate of the change of the distribution function, $\frac{\partial u}{\partial t}$, is equal to the sum of the change rates due to external forces, $\left(\frac{\partial u}{\partial t}\right)_{force}$, advection of the particles, $\left(\frac{\partial u}{\partial t}\right)_{advec}$, and particle-to-particle and particle-to-matter collisions, $\left(\frac{\partial u}{\partial t}\right)_{coll}$ [2].

For neutral particle transport, the following assumptions [3] about the behavior of the radiation particles can be utilized:

1. Particles may be considered as points;

2. Particles do not interact with other particles;

3. Particles interact with material target atoms in a binary manner;

4. Collisions between particles and material target atoms are instantaneous;

5. Particles do not experience any external force fields (*e.g.* gravity).

These assumptions lead to the first order form of the Boltzmann Transport Equation, which we simply call the transport equation for brevity. The remainder of the chapter is layed out as follows. Section 2.1 provides the general form of the neutron transport equation with some variants. Section 2.2 describes how we discretize the transport equation in energy with the multigroup methodology and Section 2.3 presents the angular discretization via collocation. Section 2.4 will conclude our discretization procedures in the spatial domain. Section 2.5 will present the iterative procedures used to converge our solution space. We then present concluding remarks for the chapter in Section 2.6.

2.1 The Neutron Transport Equation

The time-dependent neutron angular flux, $\Psi(\vec{r}, E, \vec{\Omega}, t)$, at spatial position $\vec{r}$, with energy E moving in direction $\vec{\Omega}$ and at time t, is defined within an open, convex spatial domain $\mathcal{D}$, with boundary, $\partial\mathcal{D}$ by the general neutron transport equation:

$$\begin{aligned}\frac{\partial\Psi}{\partial t} + \vec{\Omega}\cdot\vec{\nabla}\Psi(\vec{r}, E, \vec{\Omega}, t) + \sigma_t(\vec{r}, E, t)\Psi(\vec{r}, E, \vec{\Omega}, t) &= Q_{ext}(\vec{r}, E, \vec{\Omega}, t) \\ &+ \frac{\chi(\vec{r}, E, t)}{4\pi}\int dE'\nu\sigma_f(\vec{r}, E', t)\int d\Omega'\Psi(\vec{r}, E', \vec{\Omega}', t) \\ &+ \int dE'\int d\Omega'\sigma_s(E'\to E, \Omega'\to\Omega)\Psi(\vec{r}, E', \vec{\Omega}')\end{aligned} \tag{2.2}$$

with the following, general boundary condition:

$$\Psi(\vec{r}, E, \vec{\Omega}, t) = \Psi^{inc}(\vec{r}, E, \vec{\Omega}, t) + \int dE'\int d\Omega'\gamma(\vec{r}, E'\to E, \vec{\Omega}'\to\vec{\Omega}, t)\Psi(\vec{r}, E', \vec{\Omega}', t)$$
$$\text{for } \vec{r}\in\partial\mathcal{D}^-\left\{\partial\mathcal{D}, \vec{\Omega}'\cdot\vec{n} < 0\right\}. \tag{2.3}$$

In Eqs. (2.2) and (2.3), the physical properties of the system are defined as the following: $\sigma_t(\vec{r}, E, t)$ is the total neutron cross section, $\chi(\vec{r}, E, t)$ is the neutron fission spectrum, $\sigma_f(\vec{r}, E', t)$ is the fission cross section, $\nu(\vec{r}, E', t)$ is the average number of neutroncs emitted per fission, $\sigma_s(E' \to E, \Omega' \to \Omega, t)$ is the scattering cross section, and $Q_{ext}(\vec{r}, E, \vec{\Omega}, t)$ is a distributed external source.

We can simplify Eq. (2.2) to:

$$\frac{\partial \Psi}{\partial t} + \mathbf{L}\Psi = \mathbf{F}\Psi + \mathbf{S}\Psi + \mathbf{Q}, \tag{2.4}$$

by dropping the dependent variable parameters and using the following operators:

$$\begin{aligned}
\mathbf{L}\Psi &= \vec{\Omega} \cdot \vec{\nabla}\Psi(\vec{r}, E, \vec{\Omega}, t) + \sigma_t(\vec{r}, E, t)\Psi(\vec{r}, E, \vec{\Omega}, t), \\
\mathbf{F}\Psi &= \frac{\chi(\vec{r}, E, t)}{4\pi} \int dE' \nu\sigma_f(\vec{r}, E', t) \int d\Omega' \Psi(\vec{r}, E', \vec{\Omega}', t), \\
\mathbf{S}\Psi &= \int dE' \int d\Omega' \sigma_s(E' \to E, \Omega' \to \Omega, t)\Psi(\vec{r}, E', \vec{\Omega}', t), \\
\mathbf{Q} &= Q_{ext}(\vec{r}, E, \vec{\Omega}, t),
\end{aligned} \tag{2.5}$$

where $\mathbf{L}$ is the loss operator which includes total reaction and streaming, $\mathbf{F}$ is the fission operator, and $\mathbf{S}$ is the scattering operator. If we wish to analyze a transport problem at steady-state conditions, we simply drop the temporal derivative to form

$$\mathbf{L}\Psi = \mathbf{F}\Psi + \mathbf{S}\Psi + \mathbf{Q}, \tag{2.6}$$

and note that the operators of Eq. (2.5) no longer depend on time, t.

There is a special subset of transport problems that is routinely analyzed to determine the neutron behavior of a fissile system called the *k-eigenvalue problem*. In Eq. (2.2), $\nu(\vec{r}, E)$ acts as a multiplicative factor on the number of neutrons emitted per fission event. We replace this multiplicative factor in the following manner:

$$\nu(\vec{r}, E) \rightarrow \frac{\tilde{\nu}(\vec{r}, E)}{k}, \tag{2.7}$$

where we have introduced the eigenvalue, k. By also dropping the external source term, the steady-state neutron transport equation in Eq. (2.6) can be rewritten into

$$(\mathbf{L} - \mathbf{S})\,\tilde{\Psi} = \frac{1}{k}\mathbf{F}\tilde{\Psi}, \tag{2.8}$$

where $(k, \tilde{\Psi})$ forms an appropriate eigenvalue-eigenvector pair. Of most interest is the eigenpair corresponding to the eigenvalue of largest magnitude.

We can then gain knowledge of the behavior of the neutron population in the problem by taking the full phase-space integrals of the loss operator $\int\int\int \mathbf{L}\tilde{\Psi}\, dE\, d\Omega\, d\vec{r}$, the fission operator $\int\int\int \mathbf{F}\tilde{\Psi}\, dE\, d\Omega\, d\vec{r}$, and the scattering operator $\int\int\int \mathbf{S}\tilde{\Psi}\, dE\, d\Omega\, d\vec{r}$. With the appropriate eigenvector solution, $\tilde{\Psi}$, the k eigenvalue then has the meaning as the multiplicative value which balances Eq. (2.8) in an integral sense. This means that k also has a physical meaning as well. A value $k < 1$ is called subcritical and corresponds to a system whose neutron population decreases in time; a value $k = 1$ is called critical and corresponds to a system whose neutron population remains constant in time; and a value $k > 1$ is called supercritical and corresponds to a system whose neutron population increases in time [4].

2.2 Energy Discretization

We begin our discretization procedures by focusing on the angular flux's energy variable. An ubiquitous energy discretization procedure in the transport community is the multigroup method [5, 6]. The multigroup method is defined by splitting the angular flux solution into G number of distinct, contiguous, and non-overlapping energy intervals called groups. We begin by restricting the full energy domain, $[0, \infty)$,

into a finite domain, $E \in [E_G, E_0]$. E_0 corresponds to some maximum energy value and E_G corresponds to some minimum energy value (typically 0). We have done this by defining $G+1$ discrete energy values that are in a monotonically continuous reverse order: $E_G < E_{G-1} < \ldots < E_1 < E_0$.

From this distribution of energy values, we then say that a particular energy group, g, corresponds to the following energy interval:

$$\Delta E_g \in [E_g, E_{g-1}]. \tag{2.9}$$

Figure 2.1 provides a visual representation between the $G+1$ discrete energy values and the G energy groups. While the order that we have prescribed may seem illogical (high-to-low), it has been historically applied this way because radiation transport problems are iteratively solved from high energy to low energy. If the group structure is well chosen, then the transport solution can be more efficiently and easily obtained with this high-to-low energy group structure.

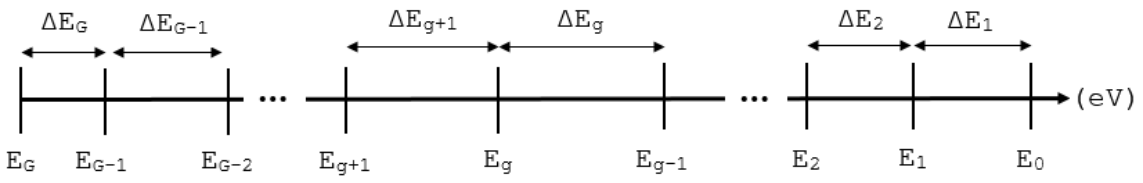

Figure 2.1: Interval structure of the multigroup methodology.

For the remainder of this energy discretization procedure, we will utilize the steady-state form of the transport equation in Eq. (2.6). The time-dependent and eigenvalue forms are analagous and would be derived identically. Taking the energy interval for group g as defined in Eq. (2.9), the energy-integrated angular flux of

group g is

$$\Psi_g(\vec{r},\vec{\Omega}) = \int_{E_g}^{E_{g-1}} \Psi(\vec{r},E,\vec{\Omega})\,dE. \tag{2.10}$$

We can then use the energy-integrated angular flux to form the following coupled, $(g = 1, ..., G)$, discrete equations (we have dropped the spatial parameter and some of the angular parameters for further clarity):

$$\left(\vec{\Omega}\cdot\vec{\nabla} + \sigma_{t,g}\right)\Psi_g = \sum_{g'=1}^{G}\left[\frac{\chi_g}{4\pi}\nu\sigma_{f,g'}\int_{4\pi}\Psi_{g'}(\vec{\Omega}')\,d\Omega' + \int_{4\pi}\sigma_s^{g'\to g}(\vec{\Omega}',\vec{\Omega})\Psi_{g'}(\vec{\Omega}')\,d\Omega'\right] + Q_g \tag{2.11}$$

where

$$\begin{aligned}
\sigma_{t,g}(\vec{r},\vec{\Omega}) &\equiv \frac{\int_{E_g}^{E_{g-1}}\sigma_t(\vec{r},\vec{\Omega},E)\Psi(\vec{r},\vec{\Omega},E)\,dE}{\int_{E_g}^{E_{g-1}}\int_{4\pi}\Psi(\vec{r},\vec{\Omega},E)\,dE} \\
\nu\sigma_{f,g}(\vec{r}) &\equiv \frac{\int_{E_g}^{E_{g-1}}\nu\sigma_f(\vec{r},E)\int_{4\pi}\Psi(\vec{r},\vec{\Omega},E)\,dEd\Omega}{\int_{E_g}^{E_{g-1}}\int_{4\pi}\Psi(\vec{r},\vec{\Omega},E)\,dEd\Omega} \\
\chi_g &\equiv \int_{E_g}^{E_{g-1}}\chi(\vec{r},E)\,dE \\
\sigma_s^{g'\to g}(\vec{r},\vec{\Omega}',\vec{\Omega}) &\equiv \frac{\int_{E_{g'}}^{E_{g'-1}}\left[\int_{E_g}^{E_{g-1}}\sigma_s(\vec{r},E'\to E,\vec{\Omega}',\vec{\Omega})\,dE\right]\Psi(\vec{r},\vec{\Omega}',E')\,dE'}{\int_{E_g}^{E_{g-1}}\Psi(\vec{r},\vec{\Omega},E)\,dE} \\
Q_g(\vec{r},\vec{\Omega}) &\equiv \int_{E_g}^{E_{g-1}}Q(\vec{r},\vec{\Omega},E)\,dE
\end{aligned} \tag{2.12}$$

The above equations are mathematically exact to those presented in Eqs. (2.2 - 2.6) and we have made no approximations at this time. However, this requires full knowledge of the energy distribution of the angular flux solution at all positions in our problem domain since we weight the multigroup cross sections with this solution.

This is obviously impossible since the energy distibution is part of the solution space we are trying to solve for. Instead, we now define the process to make the multigroup discretization an effective approximation method.

We first define an approximate angular flux distribution for a region s:

$$\Psi(\vec{r},\vec{\Omega},E) = \hat{\Psi}(\vec{r},\vec{\Omega})f_s(E), \tag{2.13}$$

which is a factorization of the angular flux solution into a region-dependent energy function, $f_s(E)$, and a spatially/angularly dependent function, $\hat{\Psi}(\vec{r},\vec{\Omega})$. With this approximation, we can redefine the energy-collapsed cross sections of Eq. (2.12):

$$\begin{aligned}
\sigma_{t,g}(\vec{r},\vec{\Omega}) &\equiv \frac{\int_{E_g}^{E_{g-1}} \sigma_t(\vec{r},\vec{\Omega},E)f_s(E)\,dE}{\int_{E_g}^{E_{g-1}} f_s(E)\,dE}, \\
\nu\sigma_{f,g}(\vec{r}) &\equiv \frac{\int_{E_g}^{E_{g-1}} \nu\sigma_f(\vec{r},E)f_s(E)\,dE}{\int_{E_g}^{E_{g-1}} f_s(E)\,dE}, \\
\sigma_s^{g'\to g}(\vec{r},\vec{\Omega}',\vec{\Omega}) &\equiv \frac{\int_{E_{g'}}^{E_{g'-1}} \left[\int_{E_g}^{E_{g-1}} \sigma_s(\vec{r},E'\to E,\vec{\Omega}',\vec{\Omega})\,dE\right] f_s(E')\,dE'}{\int_{E_g}^{E_{g-1}} f_s(E)\,dE}.
\end{aligned} \tag{2.14}$$

It is noted that we do not need to redefine the fission spectrum or the distributed external sources since they are not weighted with the angular flux solution. With this energy factorization, we would expect, in general, that the approximation error will tend to zero as the number of discrete energy groups increases (thereby making the energy bins thinner). This is especially true if the group structure is chosen with many more bins in energy regions with large variations in the energy solution. For certain problems, the region-dependent energy function is well understood (*i.e.* almost exactly known). This means, that for these problems, we can achieve reasonable solution accuracy with only a few groups where the energy bins

of the multigroup discretization are well chosen. A good example of these kinds of problems are thermal-spectrum nuclear reactors which have historically achieved reasonable solutions with as few as 4-10 energy groups.

2.3 Angular Discretization

Now that we have provided the discretization of the energy variable, we next focus on the discretization of the transport problem in angle. We will do this in two stages: 1) expand the angular flux in the scattering source and the distributed external source in spherical harmonics and 2) collocate the angular flux at the interpolation points of the trial space. We will perform these discretization procedures by taking the stready-state equation presented in Eq. (2.6), dropping the fission term and spatial parameterization, and using only 1 energy group:

$$\vec{\Omega} \cdot \vec{\nabla} \Psi(\vec{\Omega}) + \sigma_t \Psi(\vec{\Omega}) = \int_{4\pi} d\Omega' \, \sigma_s(\vec{\Omega}' \cdot \vec{\Omega}) \Psi(\vec{\Omega}') + Q(\vec{\Omega}). \tag{2.15}$$

We first expand the angular flux, scattering cross section and external source in spherical harmonics:

$$\begin{aligned} \Phi_{p,n} &\equiv \int_{4\pi} d\Omega \, \Psi(\vec{\Omega}) \, Y_{p,n}(\vec{\Omega}) \\ \sigma_{s,p} &\equiv \int_{-1}^{1} d\mu \, \sigma_s(\mu) P_p(\mu) \\ Q_{p,n} &\equiv \end{aligned} \tag{2.16}$$

where we have used the following relationships:

$$\begin{aligned} \mu &\equiv \vec{\Omega}' \cdot \vec{\Omega} \\ \sigma_s(\vec{\Omega}' \cdot \vec{\Omega}) &\equiv \frac{1}{2\pi} \sigma_s(\mu) \\ P_p(\vec{\Omega}' \cdot \vec{\Omega}) &\equiv \frac{1}{2\pi} P_p(\mu) \end{aligned} \tag{2.17}$$

Table 2.1: 2D angle mapping from the first quadrant into the other 3 quadrants.

Quadrant	μ	η
1	$\mu_1 = \mu_1$	$\eta_1 = \eta_1$
2	$\mu_2 = -\mu_1$	$\eta_2 = \eta_1$
3	$\mu_3 = -\mu_1$	$\eta_3 = -\eta_1$
4	$\mu_4 = \mu_1$	$\eta_4 = -\eta_1$

Table 2.2: 3D angle mapping from the first octant into the other 7 octants.

Quadrant	μ	η	ξ
1	$\mu_1 = \mu_1$	$\eta_1 = \eta_1$	$\xi_1 = \xi_1$
2	$\mu_2 = -\mu_1$	$\eta_2 = \eta_1$	$\xi_2 = \xi_1$
3	$\mu_3 = -\mu_1$	$\eta_3 = -\eta_1$	$\xi_3 = \xi_1$
4	$\mu_4 = \mu_1$	$\eta_4 = -\eta_1$	$\xi_4 = \xi_1$
5	$\mu_5 = \mu_1$	$\eta_5 = \eta_1$	$\xi_5 = -\xi_1$
6	$\mu_6 = -\mu_1$	$\eta_6 = \eta_1$	$\xi_6 = -\xi_1$
7	$\mu_7 = -\mu_1$	$\eta_7 = -\eta_1$	$\xi_7 = -\xi_1$
8	$\mu_8 = \mu_1$	$\eta_8 = -\eta_1$	$\xi_8 = -\xi_1$

We conclude our discussion of angular discretizations by presenting two common angular quadrature sets that will be employed in this dissertation work. Section 2.3.1 presents the Level Symmetric (LS) quadrature set and Section 2.3.2 presents the Product Gauss-Legendre-Chebyshev (PGLC) quadrature set.

2.3.1 Level-Symmetric Quadrature Set

The first quadrature set we present is the common Level Symmetric set.

2.3.2 Product Gauss-Legendre-Chebyshev Quadrature Set

The second angular quadrature set we will present is a Product Gauss-Legendre-Chebyshev (PGLC) set. It is formed by the product-wise multiplication of a Gauss-Chebyshev quadrature in the azimuthal direction and a Gauss-Legendre quadrature

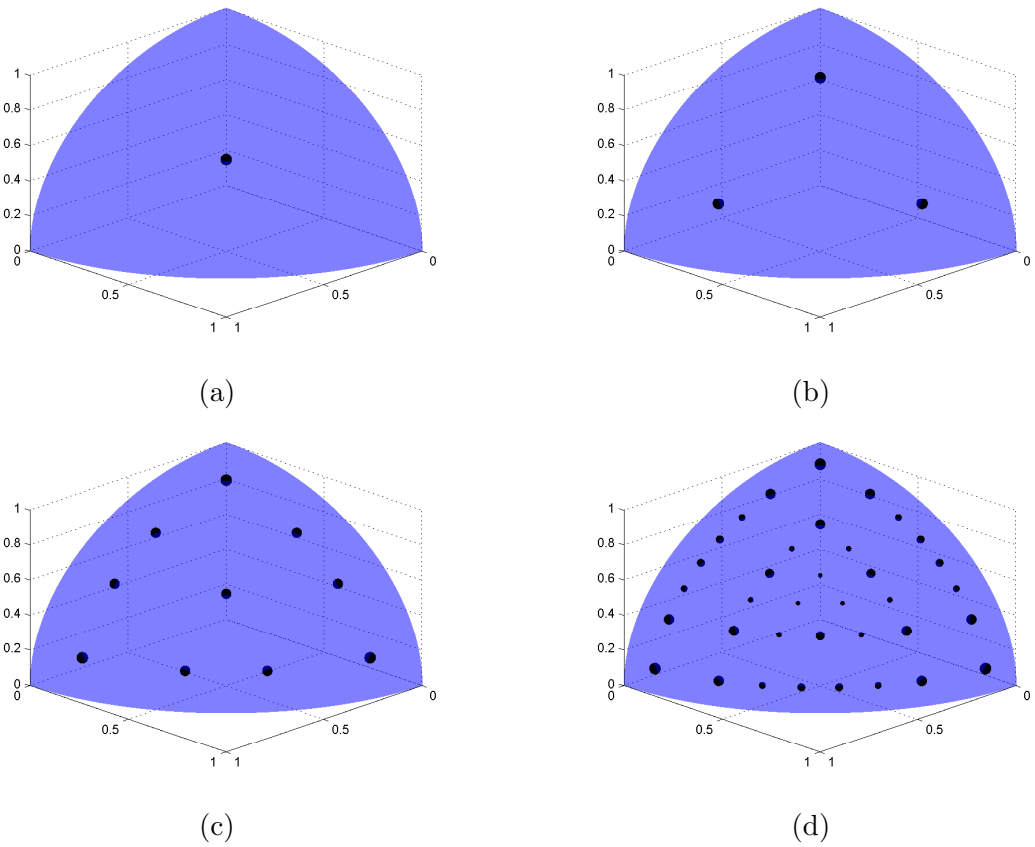

Figure 2.2: Level-Symmetric angular quadrature set of order (a) 2, (b) 4, (c) 8, and (d) 16.

in the polar direction. It has the following key differences from the Level Symmetric set:

- Does not have 90^o rotational invariance within the primary octant; still maintains octant-to-octant symmetry however;
- Has more control over the placement of the anglular directions within the primary octant;
- Quadrature weights are aligned with the polar level;
- Has strictly positive weights for all polar and azimuthal combinations.

From the listed differences, we can already discern some clear advantages and disadvantages from a fully-symmetric quadrature set like LS. If a high number of angles are required for a problem, then negative weights do not arise. Also, if the transport solution is smoothly varying in either the polar or azimuthal directions,

2.4 Spatial Discretization

Using the energy and angular discretizations presented in Sections 2.2 and 2.3, respectively, we write the standard, steady-state, multigroup S_N transport equation for one angular direction, m, and one energy group, g:

$$\left(\vec{\Omega}_m \cdot \vec{\nabla} + \sigma_{t,g}\right) \Psi_{m,g} = \sum_{g'=1}^{G} \sum_{p=0}^{N_P} \frac{2p+1}{4\pi} \sigma_{s,p}^{g' \to g} \sum_{n=-p}^{p} \Phi_{p,n,g'} Y_{p,n}(\vec{\Omega}_m) + \frac{\chi_g}{4\pi} \sum_{g'=1}^{G} \nu\sigma_{f,g'} \Phi_{g'} + Q_{m,g} \quad , \tag{2.18}$$

where we have dropped the spatial parameter for clariy and is beholden to the following general, discretized boundary condition:

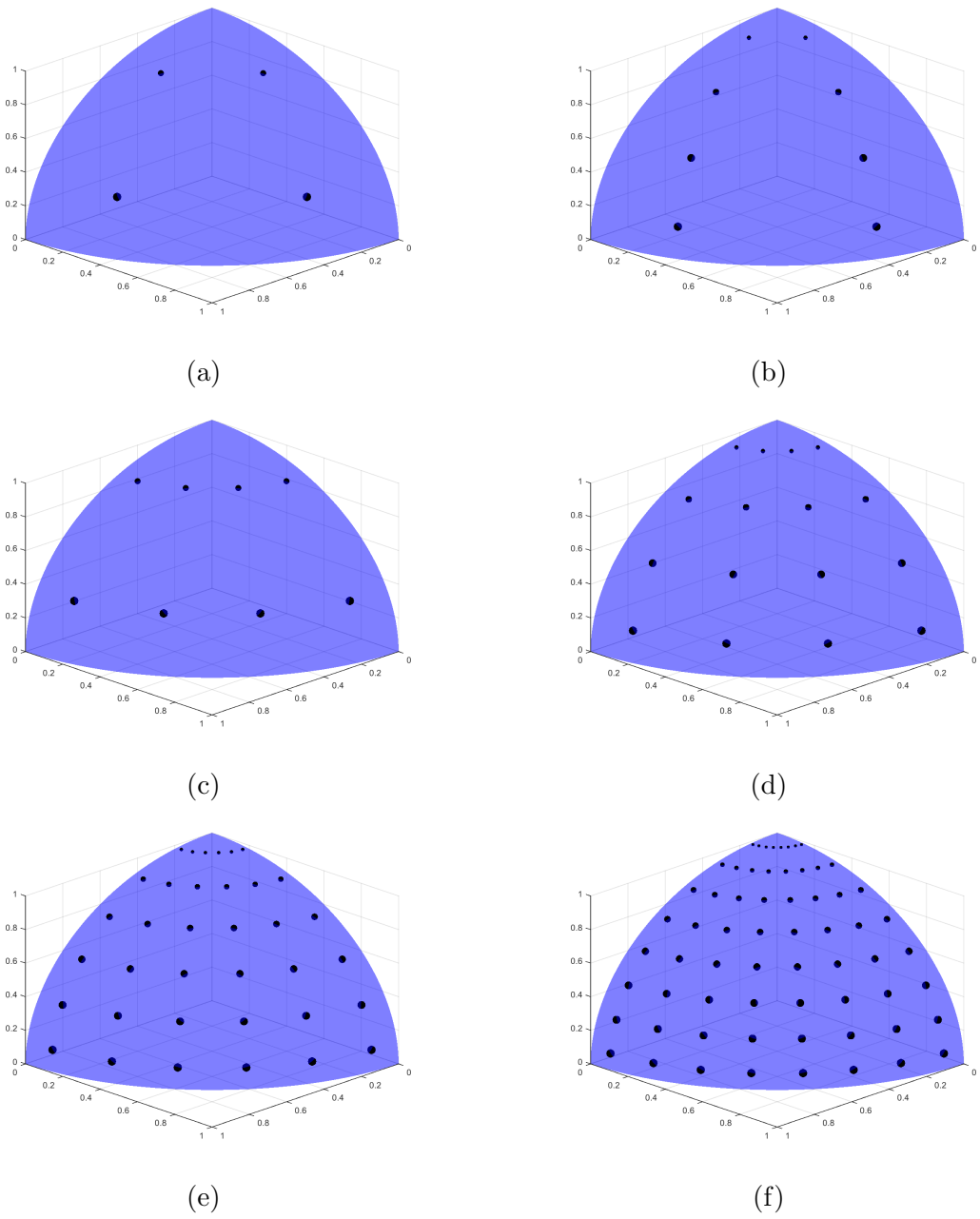

Figure 2.3: Product Gauss-Legendre-Chebyshev angular quadrature set with orders: (a) PGLC_2^2, (b) PGLC_2^4, (c) PGLC_4^2, (d) PGLC_4^4, (e) PGLC_6^6, and (f) PGLC_8^8.

$$\Psi_{m,g}(\vec{r}) = \Psi^{inc}_{m,g}(\vec{r}) + \sum_{g'=1}^{G} \sum_{\vec{\Omega}_{m'} \cdot \vec{n} > 0} \gamma^{m' \to m}_{g' \to g}(\vec{r}) \Psi_{m',g'}(\vec{r}). \tag{2.19}$$

These (MxG) number of discrete, tightly-coupled equations are currently defined as continuous in space.

For this dissertation work, we will consider only one type of boundary conditions: Dirichlet-type boundaries (also called *first-type boundary condition* in some physics and mathematical communities). In particular we will only utilize incoming-incident and reflecting boundary conditions which correspond to $\vec{r} \in \partial\mathcal{D}^d$ and $\vec{r} \in \partial\mathcal{D}^r$, respectively. The full domain boundary is then the union: $\partial\mathcal{D} = \partial\mathcal{D}^d \cup \partial\mathcal{D}^r$. This leads to the boundary condition being succinctly written for one angular direction, m, and one energy group, g as

$$\Psi_{m,g}(\vec{r}) = \begin{cases} \Psi^{inc}_{m,g}(\vec{r}), & \vec{r} \in \partial\mathcal{D}^d \\ \Psi_{m',g}(\vec{r}), & \vec{r} \in \partial\mathcal{D}^r \end{cases} \tag{2.20}$$

where the reflecting angle is $\vec{\Omega}_{m'} = \vec{\Omega}_m - 2\left(\vec{\Omega}_m \cdot \vec{n}\right)\vec{n}$ and $\vec{n}$ is oriented outward from the domain. To properly utilize the reflecting boundary condition that we have proposed, the angular quadrature set defined in Section 2.3 needs the following properties.

1. The reflected directions, $\vec{\Omega}_{m'}$, are also in the quadrature set for all $\vec{r} \in \partial\mathcal{D}^r$.

2. The weights of the incident, w_m, and reflected, $w_{m'}$, angles must be equal.

For problems where the reflecting boundaries align with the x, y, z axes, this will not be an issue with standard quadrature sets (*e.g.* level-symmetric or Gauss-Legendre-Chebyshev). However, if the reflecting boundaries do not align in this manner, then additional care must be employed in calculating appropriate angular quadrature sets.

For the spatial discretization of the problem domain, we simplify Eq. (2.18) into a single energy group and drop the fission term (it can be lumped into the 0th order external source term and will act similarly to the total interaction term)

$$\vec{\Omega}_m \cdot \vec{\nabla}\Psi_m + \sigma_t \Psi_m = \sum_{p=0}^{N_P} \frac{2p+1}{4\pi} \sum_{n=-p}^{p} Y_{p,n}(\vec{\Omega}_m) \left[\sigma_{s,p}\Phi_{p,n,} + Q_{p,n}\right] \tag{2.21}$$

to form M $(m = 1, ..., M)$ angularly discrete equations. We then lay down an unstructured mesh $\mathcal{T}_h \in \mathbb{R}^d$, over the spatial domain, where d is the dimensionality of the problem $(d = 1, 2, 3)$. This mesh consists of non-overlapping spatial elements to form a complete union over the entire spatial domain: $\mathcal{D} = \bigcup_{K \in \mathcal{T}_h} K$. To form the DGFEM set of equations [7, 8], we consider a spatial cell $K \in \mathbb{R}^d$ which has N_V^K vertices and N_f^K faces. Each face of cell K resides in dimension $\mathbb{R}^{d-1}$ and is formed by a connection of a subset of vertices. For a 1D problem, each face is a single point. For a 2D problem, each face is a line segment connecting two distinct points. For a 3D problem, each face is a $\mathbb{R}^2$ closed polygon (not necessarily coplanar) which may or not be convex. An example of this interconnection between elements is given for a $\mathbb{R}^2$ problem in Figure 2.4 between our cell of interest, K, and another cell, K', separated by the face f. We have chosen the normal direction of the face to have orientation from cell K to cell K' while we form the DGFEM equations for cell K. This means that if we were instead analyzing cell K', then the face f normal, $\vec{n}'$, would be opposite (*i.e.* $\vec{n}' = -\vec{n}$).

Next, we left-multiply Eq. (2.21) by an appropriate test function b_m, integrate over cell K, and apply Gauss' Divergence Theorem to the streaming term to obtain the Galerkin weighted-residual for cell K for an angular direction $\vec{\Omega}_m$:

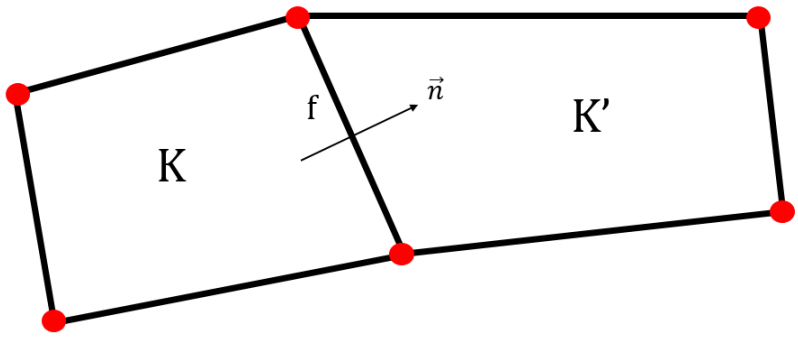

Figure 2.4: Two cells of the spatial discretization with the connecting face, f, with normal direction, $\vec{n}$, oriented from cell K to cell K'.

$$\begin{aligned} &-\left(\vec{\Omega}_m \cdot \vec{\nabla} b_m, \Psi_m\right)_K + \sum_{f=1}^{N_f^K} \left\langle \left(\vec{\Omega}_m \cdot \vec{n}\right) b_m, \tilde{\Psi}_m \right\rangle_f + \left(\sigma_t b_m, \Psi_m\right)_K \\ &= \sum_{p=0}^{N_P} \sum_{n=-p}^{p} \frac{2p+1}{4\pi} Y_{p,n}(\vec{\Omega}_m) \left[\left(\sigma_{s,p}\, b_m, \Phi_{p,n,}\right)_K + \left(b_m, Q_{p,n}\right)_K \right] \end{aligned} . \tag{2.22}$$

The cell boundary fluxes, $\tilde{\Psi}_m$, will depend on the cell boundary type and will be defined shortly. The cell boundary $\partial \mathcal{D}_K = \bigcup_{f \in N_f^K} f$ is the closed set of the N_f^K faces of the geometric cell. The inner products:

$$\left(f, g\right)_K \equiv \int_K f\, g\, dr \tag{2.23}$$

and

$$\left\langle f, g \right\rangle_f \equiv \int_f f\, g\, ds \tag{2.24}$$

correspond to integrations over the cell and faces, respectively, where $dr \in \mathbb{R}^d$ is within the cell and $ds \in \mathbb{R}^{d-1}$ is along the cell boundary. We note that we will use this

notation of the inner product for the remainder of the dissertation unless otherwise stated. We then separate the summation of the cell K boundary integration terms into two different types: outflow boundaries ($\partial K^+ = \{\vec{r} \in \partial K : \vec{n}(\vec{r}) \cdot \vec{\Omega}_m > 0\}$) and inflow boundaries ($\partial K^- = \{\vec{r} \in \partial K : \vec{n}(\vec{r}) \cdot \vec{\Omega}_m < 0\}$). The inflow boundaries can further be separated into inflow from another cell: $\partial K^- \backslash \partial \mathcal{D}$; inflow from incident flux on the domain boundary: $\partial K^- \cap \partial \mathcal{D}^d$; and reflecting domain boundaries: $\partial K^- \cap \partial \mathcal{D}^r$. At this point, we note that the derivation can comprise an additional step by using Gauss' Divergence Theorem again on the streaming term. This is sometimes performed for radiation transport work but we will not do so here. Therefore, with the cell boundary terminology as proposed, Eq. (2.22) can be written into the following form:

$$\begin{aligned} &- \left(\vec{\Omega}_m \cdot \vec{\nabla} b_m, \Psi_m\right)_K + \left(\sigma_t b_m, \Psi_m\right)_K \\ &+ \left\langle \left(\vec{\Omega}_m \cdot \vec{n}\right) b_m, \tilde{\Psi}_m \right\rangle_{\partial K^+} + \left\langle \left(\vec{\Omega}_m \cdot \vec{n}\right) b_m, \tilde{\Psi}_m \right\rangle_{\partial K^- \backslash \partial \mathcal{D}} \\ &+ \left\langle \left(\vec{\Omega}_m \cdot \vec{n}\right) b_m, \tilde{\Psi}_m \right\rangle_{\partial K^- \cap \partial \mathcal{D}^d} + \left\langle \left(\vec{\Omega}_m \cdot \vec{n}\right) b_m, \tilde{\Psi}_m \right\rangle_{\partial K^- \cap \partial \mathcal{D}^r} \\ &= \sum_{p=0}^{N_P} \sum_{n=-p}^{p} \frac{2p+1}{4\pi} Y_{p,n}(\vec{\Omega}_m) \left[\left(\sigma_{s,p}\, b_m, \Phi_{p,n,}\right)_K + \left(b_m, Q_{p,n}\right)_K \right] \end{aligned} \quad . \tag{2.25}$$

We can now deal with the boundary fluxes, $\tilde{\Psi}_m$, by enforcing the ubiquitously-used *upwind scheme*. In simple nomenclature, the upwind scheme corresponds to using the angular flux values within the cell for outflow boundaries and angular flux values outside the cell for inflow boundaries. Mathematically, the upwind scheme can succinctly be written as the following for all boundary types,

$$\tilde{\Psi}_m(\vec{r}) = \begin{cases} \Psi_m^-, & \partial K^+ \\ \Psi_m^+, & \partial K^- \backslash \partial \mathcal{D} \\ \Psi_m^{inc}, & \partial K^- \cap \partial \mathcal{D}^d \\ \Psi_{m'}^-, & \partial K^- \cap \partial \mathcal{D}^r \end{cases}, \tag{2.26}$$

when the following trace is applied to the angular fluxes :

$$\Psi_m^{\pm}(\vec{r}) \equiv \lim_{s \to 0^{\pm}} \Psi_m\Big(\vec{r} + s(\vec{\Omega}_m \cdot \vec{n})\vec{\Omega}_m\Big). \tag{2.27}$$

This trace has the notation, with $\vec{n}$ pointing outwards from cell K, of Ψ_m^- corresponding to fluxes within the cell and Ψ_m^+ corresponding to fluxes out of the cell. Now, using the upwind scheme as previously defined, we can write our complete set of DGFEM equations for cell K as

$$\begin{aligned} &-\Big(\vec{\Omega}_m \cdot \vec{\nabla} b_m, \Psi_m\Big)_K + \Big(\sigma_t b_m, \Psi_m\Big)_K + \Big\langle (\vec{\Omega}_m \cdot \vec{n})\, b_m, \Psi_m^- \Big\rangle_{\partial K^+} \\ &\quad + \Big\langle (\vec{\Omega}_m \cdot \vec{n})\, b_m, \Psi_m^+ \Big\rangle_{\partial K^- \backslash \partial \mathcal{D}} + \Big\langle (\vec{\Omega}_m \cdot \vec{n})\, b_m, \Psi_{m'}^- \Big\rangle_{\partial K^- \cap \partial \mathcal{D}^r} \\ &\quad = \sum_{p=0}^{N_P} \sum_{n=-p}^{p} \frac{2p+1}{4\pi} Y_{p,n}(\vec{\Omega}_m) \left[\Big(\sigma_{s,p}\, b_m, \Phi_{p,n,}\Big)_K + \big(b_m, Q_{p,n}\big)_K \right] \\ &\quad + \Big\langle (\vec{\Omega}_m \cdot \vec{n})\, b_m, \Psi_m^{inc} \Big\rangle_{\partial K^- \cap \partial \mathcal{D}^d} \end{aligned} \tag{2.28}$$

We note that fluxes without the trace superscript are all within the cell. By completely defining our mathematical formulation for an arbitrary spatial cell, it is easy to see that the full set of equations to define our discretized solution space for a single angle and energy group comprises of a simple double integration loop. The full set of equations can be formed by looping over all spatial cells, $\mathcal{D} = \bigcup_{K \in \mathcal{T}_h} K$, while

further looping over all faces within each cell, $\partial\mathcal{D}_K = \bigcup_{f \in N_f^K} f$. Section 2.5 will further detail how all the DGFEM equations are formed along with efficient solution methods. We conclude this section by defining the elementary matrix terms for a given cell as follows.

2.4.1 Elementary Mass Matrices

In the spatially discretized equations presented in Section 2.4, there are several reaction terms that appear with the form: $\left(\sigma b_m, \Psi_m\right)_K$ for a given angular direction, m, and for a spatial cell, K. In FEM analysis these reaction terms are ubiquitously referred to as the mass matrix terms [9, 10]. For cell K, we define the elementary mass matrix, $\mathbf{M}$ as

$$\mathbf{M}_K = \int_K \mathbf{b}_K \, \mathbf{b}_K^T \, d\vec{r}, \tag{2.29}$$

where $\mathbf{b}_K$ corresponds to the set of N_K basis functions that have non-zero measure in cell K. Depending on the FEM basis functions utilized, the integrals in Eq. (2.29) can be directly integrated analytically. However, if in general, the basis functions cannot be analytically integrated on an arbitrary set of cell shapes, then a numerical integration scheme becomes necessary. If we define a quadrature set, $\left\{\vec{x}_q, w_q^K\right\}_{q=1}^{N_q}$, for cell K, consisting of N_q points, $\vec{x}_q$, and weights, w_q^K, then we can numerically calculate the mass matrix by the following

$$\mathbf{M}_K = \sum_{q=1}^{N_q} w_q^K \mathbf{b}_K(\vec{x}_q) \, \mathbf{b}_K^T(\vec{x}_q). \tag{2.30}$$

In this case, it is necessary that the sum of the weights of this quadrature set exactly equal the geometric measure of cell K. This means that $\sum_{q=1}^{N_q} w_q^K$ is equal to the cell width in 1 dimension, the cell area in 2 dimensions, and the cell volume in 3

dimensions.

Since $\mathbf{b}_K$ consists of a column vector for the basis functions and $\mathbf{b}_K^T$ consists of a row vector, then their multiplication will obviously yield a full $(N_K \,\mathrm{x}\, N_K)$ matrix. This matrix is written for completeness of this discussion on the mass matrix:

$$\mathbf{M}_K = \begin{bmatrix} \int_K b_1\, b_1 & \dots & \int_K b_1\, b_j & \dots & \int_K b_1\, b_{N_K} \\ \vdots & & \vdots & & \vdots \\ \int_K b_i\, b_1 & \dots & \int_K b_i\, b_j & \dots & \int_K b_i\, b_{N_K} \\ \vdots & & \vdots & & \vdots \\ \int_K b_{N_K}\, b_1 & \dots & \int_K b_{N_K}\, b_j & \dots & \int_K b_{N_K}\, b_{N_K} \end{bmatrix}, \tag{2.31}$$

where an individual matrix entry is of the form:

$$M_{i,j}^K = \int_K b_i\, b_j. \tag{2.32}$$

2.4.2 Elementary Streaming Matrices

Next, we will consider the streaming term that has the form: $\left(\vec{\Omega}_m \cdot \vec{\nabla} b_m, \Psi_m\right)_K$ for a given angular direction, m, and for a spatial cell, K. $\vec{\nabla}$ is the gradient operator in physical space. It has the form of $\vec{\nabla} = \left[\frac{d}{dx}\right]$ in 1 dimension, the form of $\vec{\nabla} = \left[\frac{\partial}{\partial x}, \frac{\partial}{\partial y}\right]$ in 2 dimensions, and the form of $\vec{\nabla} = \left[\frac{\partial}{\partial x}, \frac{\partial}{\partial y}, \frac{\partial}{\partial z}\right]$ in 3 dimensions. Since for every cell, the streaming term is applied for all M angles in the angular discretization, we define the analytical elementary streaming matrix:

$$\vec{\mathbf{G}}_K = \int_K \vec{\nabla} \mathbf{b}_K\, \mathbf{b}_K^T\, d\vec{r}, \tag{2.33}$$

which has dimensionality $(N_K \mathrm{x} N_K \mathrm{x} d)$. We choose to store the elementary streaming matrix in this form and not store M separate $(N_K \mathrm{x} N_K)$ local matrices corresponding

to the application of the dot product ($\vec{\Omega}_m \cdot \int_K \vec{\nabla}\mathbf{b}_K\, \mathbf{b}_K^T\, d\vec{r}$). Instead we simply evaluate the dot product with the appropriate angular direction whenever necessary. This has great benefit when trying to run large transport problems when memory becomes a premium and processor operations are not our limiting bottleneck.

Just like the elementary mass matrix, we can use the same spatial quadrature set, $\left\{\vec{x}_q, w_q^K\right\}_{q=1}^{N_q}$, for cell K to numerically calculate the streaming matrix:

$$\vec{\mathbf{G}}_K = \sum_{q=1}^{N_q} w_q^K \vec{\nabla}\mathbf{b}_K(\vec{x}_q)\, \mathbf{b}_K^T(\vec{x}_q). \tag{2.34}$$

In this case, this local cell-wise streaming matrix has the full matrix form:

$$\vec{\mathbf{G}}_K = \begin{bmatrix} \int_K \vec{\nabla} b_1\, b_1 & \dots & \int_K \vec{\nabla} b_1\, b_j & \dots & \int_K \vec{\nabla} b_1\, b_{N_K} \\ \vdots & & \vdots & & \vdots \\ \int_K \vec{\nabla} b_i\, b_1 & \dots & \int_K \vec{\nabla} b_i\, b_j & \dots & \int_K \vec{\nabla} b_i\, b_{N_K} \\ \vdots & & \vdots & & \vdots \\ \int_K \vec{\nabla} b_{N_K}\, b_1 & \dots & \int_K \vec{\nabla} b_{N_K}\, b_j & \dots & \int_K \vec{\nabla} b_{N_K}\, b_{N_K} \end{bmatrix}, \tag{2.35}$$

where an individual matrix entry is of the form:

$$\vec{G}_{i,j}^K = \int_K \vec{\nabla} b_i\, b_j. \tag{2.36}$$

2.4.3 Elementary Surface Matrices

Finally, the last terms to consider of the discretized transport equation are those found on the faces of the cell boundary: $\vec{\Omega}_m \cdot \left\langle \vec{n}\, b_m, \Psi_m \right\rangle_{\partial K}$. These terms are analagous to the cell mass matrix but are computed on the cell boundary with dimensionality $(d-1)$.

2.5 Solution Procedures

To this point, we have properly described the procedures to discretize the transport problem in energy, angle, and space. We now spend the remainder of this chapter discussing various methodologies to efficiently solve the tightly-coupled system of equations composing our transport problem. Section 2.5.1 will discuss the different iterative procedures that can be employed to efficiently converge the angular and energy portions of the solution space and Section 2.5.2 will then discuss how we can efficiently solve the spatial portion of the solution for any given iteration.

2.5.1 Angle and Energy Iteration Procedures

2.5.2 Spatial Solution Procedures - Transport Sweeping

2.6 Conclusions

In this chapter

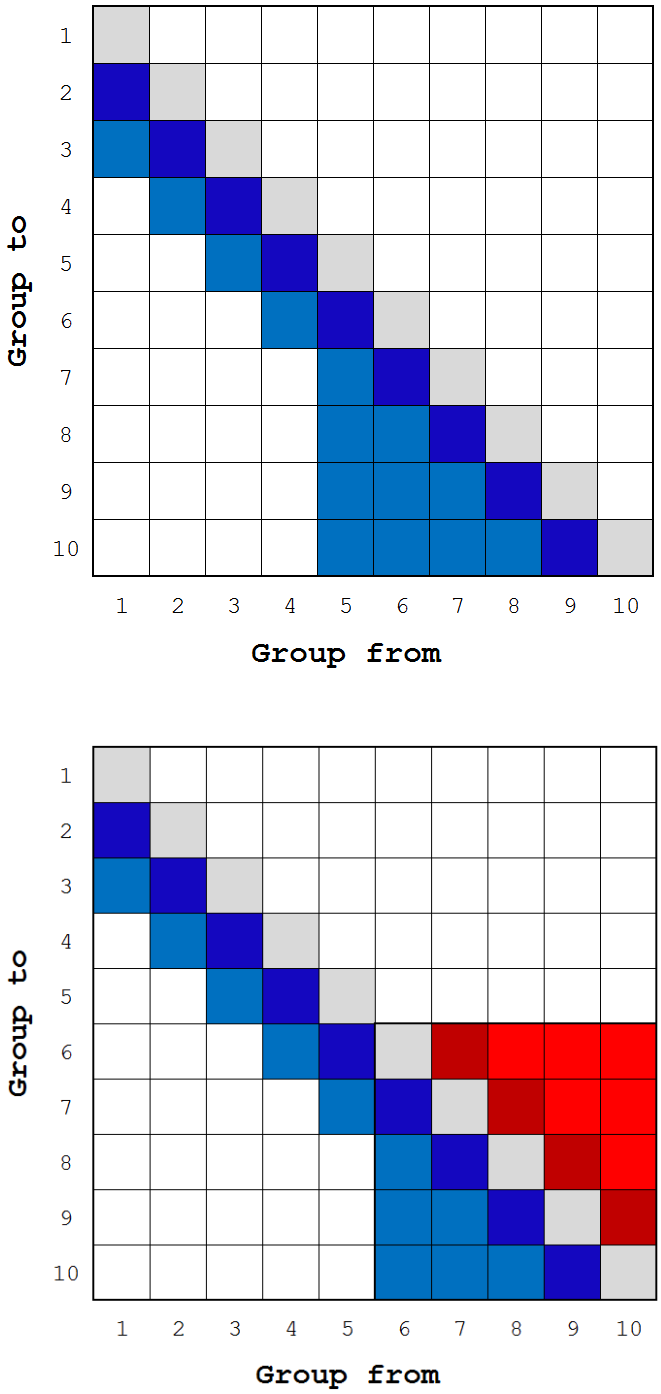

Figure 2.5: Scattering matrices (top) without and (bottom) with upscattering. The gray corresponds to within-group scattering; the blue corresponds to down-scattering in energy; and the red corresponds to up-scattering in energy.

3.1 Two-Dimensional Basis Functions on Polygons

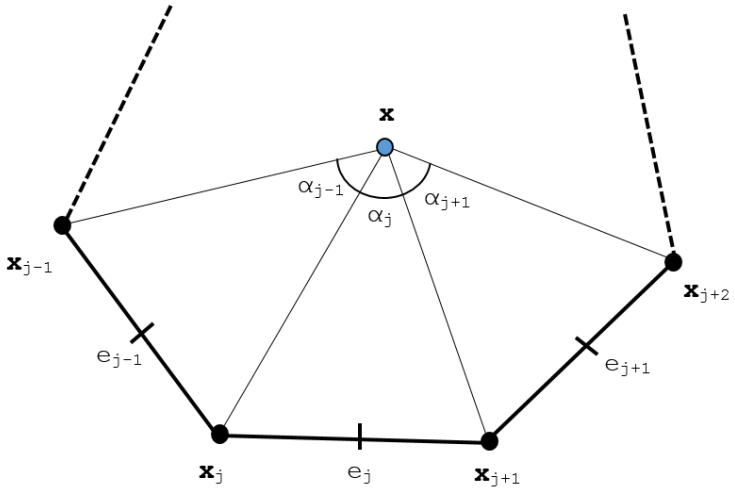

Figure 3.1: Arbitrary polygon with geometric properties used for 2D basis function generation.

3.1.1 Linearly-Complete 2D Basis Functions

In this dissertation, all 1st-order, two-dimensional basis functions for a cell will obey the properties for barycentric coordinates. They will form a *partition of unity*,

$$\sum_{i=1}^{N_K} b_i(\vec{x}) = 1; \tag{3.1}$$

coordinate interpolation will result from an *affine combination* of the vertices,

$$\sum_{i=1}^{N_K} b_i(\vec{x})\vec{x}_i = \vec{x}; \tag{3.2}$$

and they will satisfy the *Lagrange property*,

$$b_i(\vec{x}_j) = \delta_{ij}. \tag{3.3}$$

N_K is again the number of spatial degrees with measure in element K. Using the *partition of unity* of Eq. (3.1), we can rewrite Eqs. (3.1-3.2) into a separate, compact, vectorized form for completeness

$$\sum_{i=1}^{N_K} b_i(\vec{x})\vec{c}_{i,1}(\vec{x}) = \vec{q}_1, \tag{3.4}$$

where $\vec{c}_{i,1}(\vec{x})$ and $\vec{q}_1$ are the lineary-complete constraint and equivalence terms, respectively. These terms are simply:

$$\vec{c}_{i,1}(\vec{x}) = \begin{bmatrix} 1 \\ x_i - x \\ y_i - y \end{bmatrix} \quad \text{and} \quad \vec{q}_1 = \begin{bmatrix} 1 \\ 0 \\ 0 \end{bmatrix}, \tag{3.5}$$

respectively.

3.1.1.1 Linear and BiLinear Basis Functions

Before presenting basis function sets applicable to polytope finite elements, we first provide two basis functions that are exact

$$\begin{aligned} b_1(r,s) &= 1 - r - s \\ b_2(r,s) &= r \\ b_3(r,s) &= s \end{aligned} \tag{3.6}$$

and

$$
\begin{aligned}
b_1(r,s) &= (1-r)(1-s) \\
b_2(r,s) &= r(1-s) \\
b_3(r,s) &= rs \\
b_4(r,s) &= (1-r)s
\end{aligned}
\tag{3.7}
$$

3.1.1.2 Wachspress Rational Basis Functions

3.1.1.3 Mean Value Basis Functions

3.1.1.4 Metric Basis Functions

3.1.1.5 Maximum Entropy Basis Functions

3.1.1.6 Piecewise Linear (PWL) Basis Functions

$$
b_j(x,y) = t_j(x,y) + \alpha_j^K t_c(x,y) \tag{3.8}
$$

t_j is the standard 2D linear function with unity at vertex j that linearly decreases to zero to the cell center and each adjoining vertex. t_c is the 2D cell "tent" function which is unity at the cell center and linearly decreases to zero to each cell vertex. α_j^K is the weight parameter for vertex j in cell K.

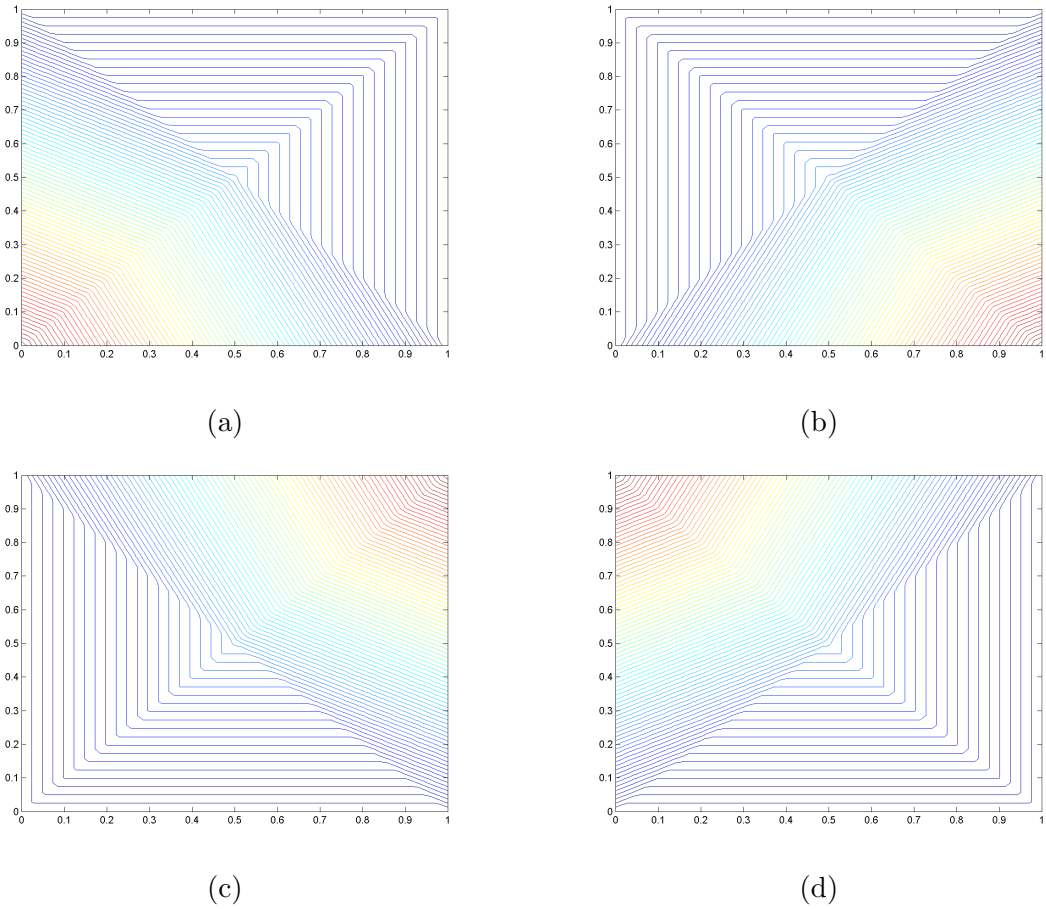

(a) (b)

(c) (d)

Figure 3.2: Contour plots of the PWL basis functions on the unit square for the vertices located at: (a) (0,0), (b) (1,0), (c) (1,1), and (d) (0,1).

3.1.1.7 Summary of Linear Basis Functions on Polygons

3.1.2 Quadratically-Complete 2D Basis Functions

$$\sum_{i=1}^{N_K} b_i(\vec{x}) = 1 \tag{3.9}$$

$$\sum_{i=1}^{N_K} b_i(\vec{x})\vec{x}_i = \vec{x} \tag{3.10}$$

$$\sum_{i=1}^{N_K}\sum_{j=1}^{N_K} \mu_{i,j}\left(\frac{\vec{x}_i \otimes \vec{x}_j + \vec{x}_j \otimes \vec{x}_i}{2}\right) = \vec{x} \otimes \vec{x} \tag{3.11}$$

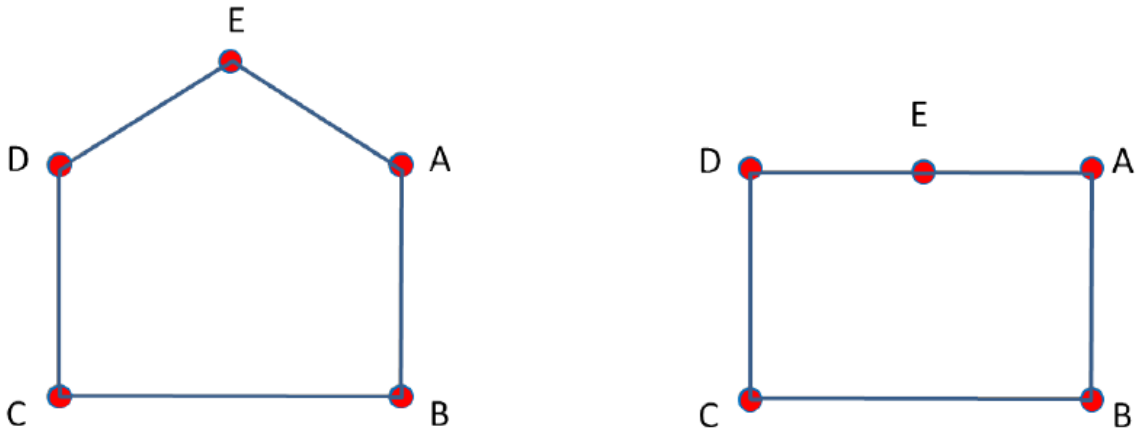

(a) (b)

Figure 3.3: Vertex structure for a (a) regular pentagonal cell and a (b) degenerate pentagonal cell.

where $\mu_{i,j}$ is a weight function corresponding to particular basis function pairings.

3.1.2.1 Serendipity Bilinear and Trilinear Basis Functions

3.2 Three-Dimensional Basis Functions on Polyhedra

3.2.1 3D Linear and TriLinear Basis Functions

$$\begin{aligned} b_1(r,s) &= 1 - r - s - t \\ b_2(r,s) &= r \\ b_3(r,s) &= s \\ b_4(r,s) &= t \end{aligned} \tag{3.12}$$

and

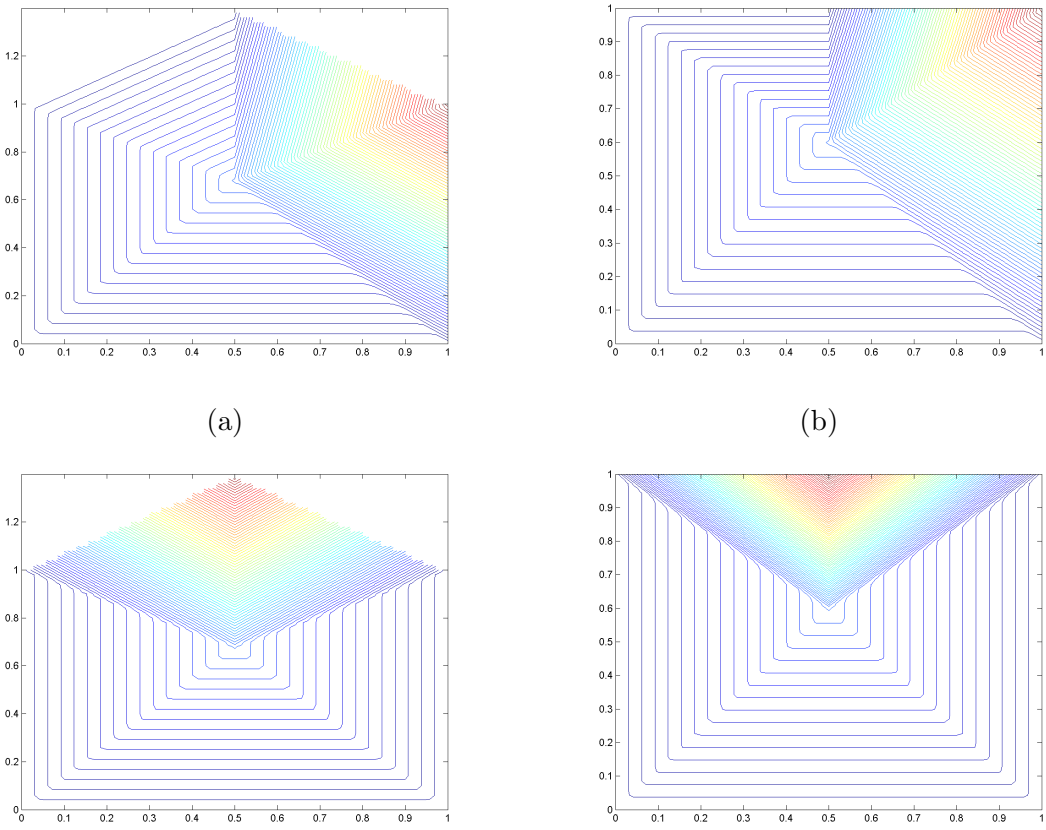

(a) (b)

(c) (d)

Figure 3.4: Contour plots of the PWL basis functions for a regular pentagon: (a) and (c) as well as a degenerate pentagon: (b) and (d).

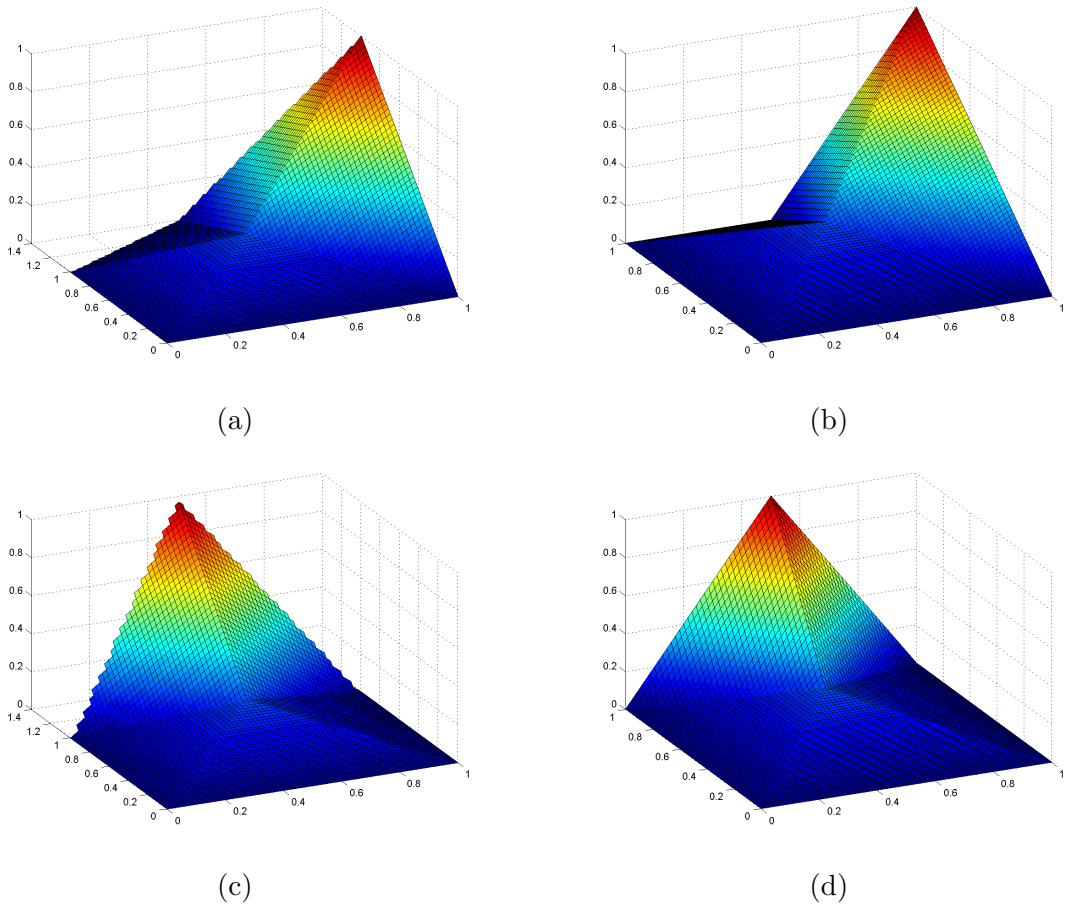

(a) (b)

(c) (d)

Figure 3.5: Plots of the PWL basis functions for a regular pentagon: (a) and (c) as well as a degenerate pentagon: (b) and (d).

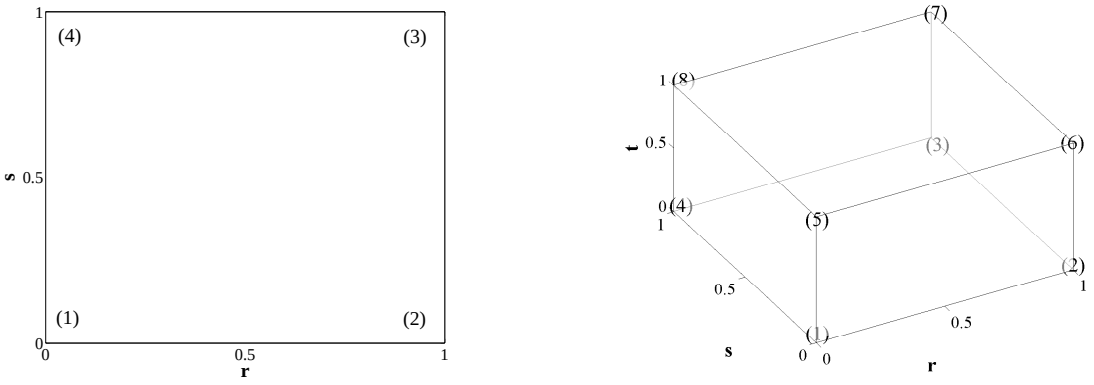

(a) (b)

Figure 3.6: Vertex structure for the (a) unit square and (b) unit cube.

$$
\begin{aligned}
b_1(r,s,t) &= (1-r)(1-s)(1-t) \\
b_2(r,s,t) &= r(1-s)(1-t) \\
b_3(r,s,t) &= rs(1-t) \\
b_4(r,s,t) &= (1-r)s(1-t) \\
b_5(r,s,t) &= (1-r)(1-s)t \\
b_6(r,s,t) &= r(1-s)t \\
b_7(r,s,t) &= rst \\
b_8(r,s,t) &= (1-r)st
\end{aligned}
\tag{3.13}
$$

3.2.2 3D Piecewise Linear (PWL) Basis Functions

The 3D PWL basis functions share a similar form to the 2D PWL basis functions.

$$
b_j(x,y,z) = t_j(x,y,z) + \sum_{f=1}^{F_j} \beta_f^j t_f(x,y,z) + \alpha_j^K t_c(x,y,z) \tag{3.14}
$$

t_j is the standard 3D linear function with unity at vertex j that linearly decreases to zero to the cell center, the face center for each face that includes vertex j, and each vertex that shares an edge with vertex j. t_c is the 3D cell "tent" function which is unity at the cell center and linearly decreases to zero to each cell vertex and face center. t_f is the face "tent" function which is unity at the face center and linearly decreases to zero at each vertex on that face and the cell center. $\beta_{f,j}$ is the weight parameter for face f touching cell vertex j, and F_j is the number of faces touching vertex j. Like the previous work defining the PWLD method [11], we also choose to assume the cell and face weighting parameters are

$$
\alpha_{K,j} = \frac{1}{N_K} \qquad \text{and} \qquad \beta_{f,j} = \frac{1}{N_f}, \tag{3.15}
$$

respectively, where N_K is the number of vertices in cell K and N_f is the number of vertices on face f, which leads to constant values of α and β for each cell and face, respectively. This assumption of the cell weight function holds for both 2D and 3D.

3.3 Numerical Results

Now that we have presented several linear polygonal finite element basis sets along with the methodology to convert them to quadratic serendipity-like basis, we present several numerical problems to demonstrate our methodology. First, we demonstrate that the presented basis sets preserve the thick diffusion limit in Section 3.3.1. Next, we present some convergence properties of the basis sets using the method of manufactured solutions (MMS) in Section 3.3.2. We then present a searchlight problem and observe how the basis sets react with adaptive mesh refinement (AMR) to mitigate numerical dispersion through a vacuum in Section 3.3.3.

3.3.1 Transport Solutions in the Thick Diffusive Limit

We present our first numerical example by demonstrating that the various polygonal finite element basis sets satisfy the thick diffusion limit.

$$\begin{aligned} \sigma_t &\rightarrow \frac{\sigma_t}{\epsilon} \\ \sigma_a &\rightarrow \epsilon\sigma_t \\ \frac{Q_0}{4\pi} &\rightarrow \epsilon\frac{Q_0}{4\pi} \end{aligned} \tag{3.16}$$

$$\vec{\Omega}\cdot\vec{\nabla}\Psi + \frac{\sigma_t}{\epsilon}\Psi = \sigma_t\left(\frac{1}{\epsilon}-\epsilon\right)\frac{\Phi}{4\pi} + \epsilon\frac{Q_0}{4\pi} \tag{3.17}$$

$$\epsilon\vec{\nabla}\cdot\frac{1}{3\sigma_t}\vec{\nabla}\Phi + \epsilon\sigma_t\Phi = \epsilon Q_0 \tag{3.18}$$

$$\begin{aligned} \vec{\Omega} \cdot \vec{\nabla} \Psi + \frac{1}{\epsilon} \Psi &= \left(\frac{1}{\epsilon} - \epsilon \right) \frac{\Phi}{4\pi} + \frac{\epsilon}{4\pi} \\ \frac{\epsilon}{3} \nabla^2 \Phi + \epsilon \Phi &= \epsilon \end{aligned} \tag{3.19}$$

3.3.2 Analytical Transport Solutions by the Method of Manufactured Solutions

The next numerical example we investigate involves the method of manufactured solutions (MMS).

3.3.3 Searchlight Problem

The next example models a beam or searchlight. Similar problems were investigated in Dedner and Vollmöller [12] and Wang and Ragusa [13]. In this problem, an incident beam of neutrons is shined onto a small portion of a boundary, propagates through a vacuum, and then exits through a small portion of a different boundary. As the beam propagates through the vacuum, the spatial discretization causes radiation outflow through all downwind cell faces. This leads to numerical dispersion and will cause to beam to artificially broaden.

In this problem, we investigate an $\mathbb{R}^2$ domain of size $[0, 1]^2$. The radiation enters the left boundary between $0.2 \leq y \leq 0.4$ with an un-normalized angular direction of $[1, 0.4]$. For this chosen direction, the radiation beam would analytically leave the right boundary between $0.6 \leq y \leq 0.8$. This means that any radiation leaving the right boundary for all other y values is due to the numerical dispersion of the beam.

We investigated this problem using several of the 2D polygonal basis functions as outlined in Section 3.1 as well as

3.4 Conclusions

In this chapter, we have presented

REFERENCES

[1] R. LERNER and G. TRIGG, *Encyclopaedia of Physics*, 2 ed. (1991).

[2] C. PARKER, *McGraw Hill Encyclopaedia of Physics*, 2 ed. (1994).

[3] J. J. DUDERSTADT and W. R. MARTIN, *Transport theory*, John Wiley & Sons (1979).

[4] K. OTT and W. BEZELLA, *Introductory Nuclear Reactor Statics*, American Nuclear Society (1989).

[5] J. J. DUDERSTADT and L. J. HAMILTON, *Nuclear reactor analysis*, Wiley (1976).

[6] E. E. LEWIS and W. F. MILLER, *Computational methods of neutron transport*, John Wiley and Sons, Inc., New York, NY (1984).

[7] A. ERN and J.-L. GUERMOND, *Theory and practice of finite elements*, vol. 159, Springer Science & Business Media (2013).

[8] T. A. WAREING, J. M. MCGHEE, J. E. MOREL, and S. D. PAUTZ, "Discontinuous finite element S_N methods on three-dimensional unstructured grids," *Nuclear science and engineering*, **138**, *3*, 256–268 (2001).

[9] O. ZEINKIEWICZ, R. TAYLOR, and J. ZHU, *The finite element method: its basis and fundamentals*, SElsevier Butterworth-Heinemann (2005).

[10] J. AKIN, *Application and implementation of finite element methods*, Academic Press, Inc. (1982).

[11] T. S. BAILEY, *The piecewise linear discontinuous finite element method applied to the RZ and XYZ transport equations*, Ph.D. thesis, Texas A&M University (2008).

[12] A. DEDNER and P. VOLLMÖLLER, "An adaptive higher order method for solving the radiation transport equation on unstructured grids," *Journal of Computational Physics*, **178**, *2*, 263–289 (2002).

[13] Y. WANG and J. C. RAGUSA, "Standard and goal-oriented adaptive mesh refinement applied to radiation transport on 2D unstructured triangular meshes," *Journal of Computational Physics*, **230**, *3*, 763–788 (2011).